Quasi-geostrophic three-dimensional flow in a cylinder

C. Macaskill
School of Mathematics and Statistics
University of Sydney
NSW 2006, Australia

December 11, 1998

Abstract

In this paper a pseudo-spectral (collocation) method is used for the problem of inviscid, quasi-geostrophic flow in a cylinder of finite vertical extent. The numerical techniques employed are described, and results are presented for a variety of initial conditions. Previous work has indicated that in two dimensions relatively simple quasi-steady final states can be obtained [11]. In this work we find similar long-time results. We also observe other long-lived states, including a tripole and a slowly precessing quadrupole, but these states eventually break down. These states tend to develop more quickly when the initial vorticity varies with depth. It is found that, for example, the analogue of a dipole in two dimensions consists of two blobs of potential vorticity of opposite sign, roughly ellipsoidal in shape and elongated in the vertical. The cross-sectional form of these final states is clearly related to the fundamental linear Bessel modes of the system, as has been noted by previous authors.

1 Introduction

In order to study vortex dynamics in the oceans and atmosphere, it is in many cases necessary to use three-dimensional models. This is due to the fact that the dominant physical mechanisms are the competing effects of rotation and stratification. In the limiting cases where one or the other effect dominates the flow does indeed become two-dimensional, i.e. for very strong rotation, the vertical shear approaches zero and the flow is completely coupled in the vertical, while in the opposite limit when stratification becomes dominant the flow at any depth is essentially independent of that at any other depth. Although these two limits have been explored extensively and give much insight into the way in which vortices are formed and interact, in reality the physical parameters are such that the intermediate case must be studied, where there is significant coupling in the vertical, but it is relatively weak. In this case one can use the well-known quasi-geostrophic model, which is the simplest model that introduces three-dimensionality in a consistent way. However, this model ignores the vertical advection of potential vorticity, and hence is inadequate if there are significant distortions of isopycnals. Despite this, many features of observed flows can be modelled in this way, and considerable numerical work has been done in the case where the horizontal boundaries are taken to be doubly periodic. Examples of pseudo-spectral methods applied to the problem with vertically periodic boundary conditions can be found in [13, 14] and contour dynamics has been used for rigid top and bottom boundary conditions in [7, 4].

However, much of the laboratory work has been carried out in rotating cylindrical tanks with rigid walls [9]. Furthermore, in recent work, [1, 12], forcing at the cylindrical wall was introduced in the form of alternating sources and sinks at a particular depth. (Note however, that in this case the tank proper was square in cross-section with the circular geometry introduced through a shallow annular collar at mid-depth, and internal to the tank, on which the sources and sinks were located.) Therefore, it is of interest to consider vortex interactions in cylindrical geometry, in particular because the effects of horizontal boundaries and of boundary forcing can then be considered while retaining a relatively simple computational domain.

In this paper a pseudo-spectral (collocation) method is described for quasi-geostrophic, inviscid flow in a circular cylinder, using a Chebyshev expansion in the radial direction and incorporating rigid lid and bottom boundary conditions. The stream-function is prescribed on the cylindrical horizontal boundary, i.e. the radial velocity is prescribed, so that a slip boundary condition is employed, corresponding to inviscid flow. It is clear that in practice one would expect the influence of viscosity to be very significant near the walls, where vorticity is generated in real flows, but it is suggested that the inviscid results presented here still have some relevance to observations. Furthermore, one finds significant ageostrophic effects in laboratory flows, so that the quasi-geostrophic approximation can be questioned, but is used here on the basis that it is the simplest model demonstrating three-dimensional phenomena in a rotating, stratified environment.

This code has been used to study some initial value problems with up to 29 vertical levels, and it has been found that there are some strong similarities with the results of Dritschel and co-workers using horizontally periodic boundaries [6, 5]). Vertical instabilities give rise to the breakup of vertically coherent vortices through very strong (turbulent) interactions, involving repeated straining out and merger of vortices, with the formation of ellipsoidal potential vorticity blobs at long times. The additional role of the cylindrical boundaries is to give rise to long-time solutions of monopolar form (a large central blob of vorticity surrounded by a weaker annulus of opposite sign), or dipolar form (the dipole moves diametrically across the cylinder, separates into opposite sign monopoles which move back around the boundary of the cylinder and then reform into a dipole, and then the sequence repeats), with radial structure very close to the corresponding linear Bessel modes. Work on a similar problem, but in two dimensions, has been reported in [11] where they used an expansion in

Bessel modes, and a no-slip boundary condition. They found similar results to those reported here in some cases: for example they identified the dipolar and monopolar modes described above as long time solutions after starting with random initial conditions, although in their case the dipole remained 'stuck' to the wall, thus creating high gradients and acting as a continuing source for the generation of vorticity. In particular they emphasised the important role of the total angular momentum, and observed that a monopolar solution, as described above, was always found at long time if the total initial angular momentum was sufficiently large; no exceptions to this general result have been found at this stage in the three-dimensional simulations performed here.

2 The quasi-geostrophic equations

We consider quasi-geostrophic flow in a circular cylinder. In cylindrical polar coordinates (r, θ, z), the quasi-geostrophic equations for the potential vorticity q and the stream-function ψ are then [17]:

$$\frac{\partial q}{\partial t} + \frac{1}{r}\left(-\frac{\partial \psi}{\partial \theta}\frac{\partial q}{\partial r} + \frac{\partial \psi}{\partial r}\frac{\partial q}{\partial \theta}\right) = D(q) \tag{1}$$

with $D(q)$ a hyperviscous term included only for numerical stability and acting only in the horizontal, and

$$\nabla_h^2 \psi + \frac{f^2}{N^2}\frac{\partial^2 \psi}{\partial z^2} = q - f. \tag{2}$$

Here the horizontal radial and transverse velocities, u and v respectively, are given by $u = -\dfrac{1}{r}\dfrac{\partial \psi}{\partial \theta}$ and $v = \dfrac{\partial \psi}{\partial r}$, and the horizontal Laplacian takes the form

$$\nabla_h^2 = \frac{1}{r}\frac{\partial}{\partial r}\left(r\frac{\partial \psi}{\partial r}\right) + \frac{1}{r^2}\frac{\partial^2 \psi}{\partial \theta^2}. \tag{3}$$

.

The buoyancy frequency N, which is constant in all the results given here, is given in general by $N(z) = \sqrt{-\dfrac{g}{\rho}\dfrac{d\rho}{dz}}$, where $\rho(z)$ is the corresponding density profile. Rotation is introduced through $f = 2\Omega$ where Ω is the constant rotation rate, which is required to be large for the quasi-geostrophic equations to be consistent. We note that the f appearing on the right hand side of the Poisson equation for the stream function can be absorbed in the definition of the potential vorticity q. The vertical boundary conditions are taken to be $\partial\psi/\partial z = 0$ at the top and bottom boundaries of the cylinder. As we are assuming an inviscid flow, on the side wall of the cylinder we take a slip boundary condition, i.e. we let v evolve freely, and specify the radial velocity u by fixing the streamfunction for all time at all points on the wall. Thus for zero radial inflow, for example, we set $\psi = 0$ on the cylinder wall.

Without loss of generality, the radius of the cylinder is at $r = 2$ and the cylinder has height $\bar{z} = \pi$ in terms of the scaled vertical coordinate $\bar{z} = z/(f/N)$. With this non-dimensionalization, we expect that a vortex in the straining field arising from a vortex of like sign will be vertically unstable if its height is more than three times its diameter [6].

3 Numerical solution of the equations

In order to solve the equations an explicit spectral collocation method is used, with a fourth order low-storage Runge-Kutta method used for the time-stepping [2]. A uniform grid is used in the vertical direction, corresponding to a cosine expansion, a standard Fourier expansion is used in azimuth and finally a Chebyshev expansion is employed in the radial direction. Radial derivatives are calculated by matrix multiplication and azimuthal derivatives are calculated using FFTs. An eighth order hyperdiffusive filter, corresponding to $D(q)$, is used in the horizontal only.

Difficulties with the coordinate singularity have been avoided using a device described in [8]. Basically, the idea is to work on a radial grid defined for both positive and *negative* radius, but with angle running only from $-\pi/2$ to $\pi/2$. The idea is effectively equivalent to that used in some earlier fully spectral codes e.g. [16], where expansions in appropriately chosen Chebyshev polynomials of the first kind were used (see also equation (3.4.3) of [2]). The horizontal grid is then given by $r \in [-2, 2]$ and $\theta \in [-\pi/2, \pi/2]$. This has two advantages. First, the radial grid points are clustered near the cylinder wall, and not at the origin, so that there is no difficulty with the coordinate singularity. Secondly, there is no requirement to specify boundary conditions at the origin and we incorporate the side boundary conditions at $r = \pm 2$ in the Chebyshev derivative matrices. The only difficulty is that one can no longer immediately use FFTs to calculate azimuthal derivatives. This problem is overcome by switching, when required, to the alternative grid $r \in (0, 1]$ and $\theta \in [-\pi, \pi)$, using the obvious relation $f(r, \theta + \pi) = f(-r, \theta)$ to construct any required function values f at the extra angles. This corresponds to

$$\tilde{f}_l(-r) = (-1)^l \tilde{f}_l(r) \tag{4}$$

where the discrete Fourier transform is

$$\tilde{f}_l(r) = \Sigma_k f(\theta_k, r) \exp i2\pi kl/L, \tag{5}$$

for any $f(\theta, r)$ evaluated at $\theta = \theta_k, k = 0, 1, \ldots, L-1$ Thus the penalty involved is the switching back and forth between the two grid representations in the horizontal, but this is a minor overhead.

A matrix decomposition technique is used to solve equation (2) at each timestep. We take the discrete Fourier transform in θ and find

$$r\frac{\partial}{\partial r}\left(r\frac{\partial \tilde{\psi}_l}{\partial r}\right) - l^2\tilde{\psi}_l + r^2\frac{\partial^2 \tilde{\psi}_l}{\partial \bar{z}^2} = r^2\tilde{q}_l. \tag{6}$$

or, if we discretize in r and $\bar{z}$, with M and N grid points respectively, we arrive at the $M \times N$ simultaneous equations in matrix notation

$$A\tilde{\psi}_l - l^2\tilde{\psi}_l + \alpha\tilde{\psi}_l B^T = \alpha\tilde{q}_l. \tag{7}$$

Here the $M \times M$ matrix A represents the radial operator $r\partial/\partial r\,(r\partial/\partial r)$, but with the first and last rows replaced by the boundary conditions at $r = \pm 2$, B^T is the transpose of the $N \times N$ matrix representing the vertical operator $\partial^2/\partial\bar{z}^2$ and α is a row vector with elements $\alpha_m = r_m^2$, $m = 0, 1, \ldots M-1$.

In a doubly periodic geometry, the operators corresponding to A and B separate, the matrices can be diagonalized once and for all, and the equation (7) can be efficiently inverted at each timestep, with only a diagonal matrix to be inverted for each different azimuthal mode. In the present case, because of the r^2 term appearing ahead of the vertical operator, one can use a similar approach, but only if full inverses are calculated once and for all and stored for each $\bar{z}$-value and for each azimuthal mode. In practice, this requires storage at N $\bar{z}$-levels and for each of $L/2+1$ azimuthal modes of an $M \times M$ real matrix inverse, which corresponds to around 16Mbytes in single precision or 33Mbytes in double precision at the resolution used here (64 radial points in $[-2, 2]$, 33 azimuthal points in $[-\pi/2, \pi/2]$ and 29 vertical levels). Thus, with a reasonable amount of memory, one could still use this approach with significantly enhanced resolution over that presently used; obviously the alternative is to recalculate the matrix inverses as required, but this is very much slower, even with good iterative methods.

4 Results

For the two-dimensional problem the following linear modes are solutions of the fully nonlinear problem (when the dissipation term is set to zero):

$$\psi_0 = J_p\left(\frac{r_0}{r_a}r\right)\begin{Bmatrix}\cos p\theta \\ \sin p\theta\end{Bmatrix} \tag{8}$$

where $J_p(r), \quad p = 0, 1, \ldots$ are Bessel functions of the first kind and

$$q_0 = -\left(\frac{r_0}{r_a}\right)^2 \psi_0 \tag{9}$$

for a cylinder of radius $r = r_a$ ($r_a = 2$ here). By suitable choice of r_0 we can impose the radial velocity at the boundary. For example, by choosing r_0 to be the first zero of $J_p(r)$ the stream function is zero there, and hence $u = -\dfrac{1}{r}\dfrac{\partial\psi}{\partial\theta}$ is also zero at the cylinder boundary. Because there is no vertical advection term in the potential vorticity equation, we can generalise these modes to construct three-dimensional solutions of the fully nonlinear problem. If we let $\psi = \psi_0 h(z)$ for any given function $h(z)$ then the Poisson equation (2) gives directly

$$q = -\left[\left(\frac{r_0}{r_a}\right)^2 - \frac{h''}{h}\right]\psi_0 \tag{10}$$

These modes, and linear combinations of them, make convenient initial conditions with suitably chosen vertical variation $h(z)$. Henceforth, we take

$$h(z) = 1 - \beta \cos 2z \tag{11}$$

where β is a constant which reduces to zero in the two-dimensional case.

First we consider the case $p = 4$, with azimuthal asymmetry introduced by perturbing with mode 1, i.e.

$$\psi_0 = 0.25 J_4(r_0^{(4)} r/2) \cos 4\theta + 0.01 J_1(r_0^{(1)} r/2) \cos \theta \tag{12}$$

where $r_0^{(4)}, r_0^{(1)}$ are chosen to be the zeros of the respective Bessel functions, thus ensuring that the radial velocity is zero at the cylinder wall. We compare the case where there is no variation in depth $\beta = 0$ with that where $\beta = 0.5$. In both cases the angular momentum (twice the volume integral of the stream function) is zero, as follows immediately given the periodic variation of the two modes in the azimuthal direction. We consider the $\beta = 0$ case first. Over the course of the calculation, the total enstrophy is reduced to about 20% of its initial level as vortices, particularly those of like sign, interact and are strained out, so creating high wavenumber structures in the horizontal. At sufficiently high wavenumber the artificial dissipation then acts to remove enstrophy. Energy, by contrast, diminishes by only about 5% as energy is predominantly shifted to larger horizontal scales (see e.g. [14] for a similar case). In figure 1 we show a time sequence of the potential vorticity. After strong interactions, with repeated merger and straining out, the final state consists of a nearly dipolar structure (very similar in form to the mode 1 perturbation) which translates across the centre of the cylinder, and then breaks up into two monopoles when it reaches the cylinder wall [3]. These monopoles then move back around the walls and reform into a dipole when they meet, after which the pattern begins again. Superposed on this repeating motion is a slow precession. Note that at this stage the enstrophy is now almost constant (see figure 2). Note also in figure 2 the sharp decreases in enstrophy. These appear to correspond to the times of greatest interaction, with major merging events taking place soon after. For example at around $t = 70$ there is a move from four to three vortices of each sign, and then at $t = 150$ from three to two, and then finally we find the final state at around $t = 240$. The three-dimensional problem ($\beta = 0.5$) shows considerable similarity to the two-dimensional one, at least at the middle depth, as indicated in the comparison of figure 3. Although some transitions in enstrophy occur earlier in the $\beta = 0.5$ case, the transition to the dipole state actually occurs slightly later. Moreover, three-dimensional contours (figure 4) show strong very strong interactions near to the top and bottom of the cylinder, leading finally to structures that although similar in cross-section to the two-dimensional case at mid-depth, have a characteristic height to diameter ratio close to 1.5 (see [13]).

As our next case, we take the initial condition as in equation (12) with $\beta = 0.5$, but now with $r_0^{(4)}$ taken to be the first maximum of $J_4(r)$. This gives zero transverse velocity at the boundary initially, and a large radial component there. Correspondingly the vorticity is maximum at the cylinder wall. We then set $\psi = 0$ at the wall for the rest of the calculation, so that an immediate adjustment in the vorticity field has to take place, with the vorticity being advected towards the centre of the cylinder. We find that this is indeed the case (see figure 5), but after the initial adjustment, behaviour similar to that observed in the previous case takes place, with the difference that a quadrupole structure persists for a considerable part of the calculation. Figure 6 shows a sequence of three-dimensional contours for this case, indicating again that the blobs of potential vorticity are roughly ellipsoidal, with a height to diameter ratio near to 1.5 .

Finally, we take the initial condition

$$\psi_0 = 0.25 J_4(r_0^{(4)} r/2)\cos 4\theta + 0.01 J_0(r_0^{(0)} r/2)\cos\theta \tag{13}$$

where again $r_0^{(4)}, r_0^{(0)}$ are chosen to be the zeros of the respective Bessel functions and where $\beta = 0.5$. The zeroth order mode used here means that the angular momentum is no longer zero. In the sequence of contour plots shown in Figure 7 we see that in this case the final state at mid-depth consists of a tripole, with a strong central monopole surrounded by two monopoles of opposite sign potential vorticity. Other runs with greater angular momentum (i.e. greater initial mode zero component) eventually gave rise to a monopole surrounded by an annulus of opposite sign, as in the two-dimensional results of [11]. It is expected that the present case would show similar behaviour at sufficiently long times. In Figure 8, the three-dimensional contours for positive potential vorticity show extreme (spiralling) interactions near to the top and bottom (see [10] for a discussion of such patterns in rotating flows), with a final state that is close to uniform over a considerable part of the depth.

5 Conclusion

In this paper we have shown that many interesting final and intermediate states arise in the simplified problem of quasi-geostrophic flow in a cylinder of finite depth. Future work can go in many directions. First, the adequacy of the quasi-geostrophic approximation must be explored. Secondly, the effects of varying the stratification profile can be studied with the code in its present form. Further work may well require much higher numerical resolution. It is expected that if the quasi-geostrophic model is retained that a contour-dynamics technique now well-established for horizontally periodic three-dimensional quasi-geostrophic flow [4] can be modified to deal with cylindrical geometry. If the slip boundary condition is set aside, and the effects of finite Reynolds number are included(see [15]), then semi-implicit methods will probably be needed to deal with the no-slip boundary condition. Finally, it is anticipated that some semi-analytical/numerical work can be done on the evolution of the attracting states described above.

6 Acknowledgments

The author gratefully acknowledges discussions on this problem with Dr D.G. Dritschel and Dr D. Broutman. The work was partially supported by the Australian Research Council. Some of this work was done while the author was on study leave at the School of Mathematics at the University of Warwick and in the School of Mathematics, University of New South Wales.

References

[1] Boubnov B.M., Dalziel S.B. & Linden P.F. Source-sink turbulence in a stratified fluid, *J. Fluid Mech.* **261** 273–303 1994.

[2] Canuto C., Hussaini M.Y., Quarteroni A. & Zang T.A. *Spectral methods in fluid dynamics*, Springer-Verlag, Berlin, 1988

[3] Carnevale G.F., Velasco Fuentes O.U. & Orlandi P Inviscid dipole-vortex rebound from a wall or coast, *J. Fluid Mech.* **351** 75–103 1997

[4] Dritschel D.G. & Ambaum M.H.P. A contour-advective semi-Lagrangian algorithm for the simulation of fine-scale conservative fields, *Q. J. Roy. Meteorol. Soc.* **123** 1097–1130 1997

[5] Dritschel D.G. & Macaskill C. On the numerical simulation of quasi-geostrophic turbulence, submitted to *Physics of Fluids* 1998

[6] Dritschel D.G. & de la Torre Juárez M. The instability and breakdown of tall columnar vortices in a quasi-geostrophic fluid, *J. Fluid Mech.* **328** 129–160 1996

[7] Dritschel D.G. & Saravanan R. Three-dimensional quasi-geostrophic contour dynamics, with an application to stratospheric vortex dynamics, *Q. J. Roy. Meteorol. Soc.* **120** 1267–1297 1994

[8] Fornberg B. A pseudo-spectral approach for polar and spherical geometries, *SIAM J. Sci. Comput.* **16** 1071–81 1995

[9] Hopfinger E.J. & van Heijst G.J.F. Vortices in rotating fluids, *Ann. Rev. Fluid Mech.* **25** 241 1993

[10] Knobloch E. Bifurcations in rotating systems *Lectures on Solar and Planetary Dynamos* Eds. M.R.E. Proctor and A.D. Gilbert Cambridge University Press, 331–372 1994

[11] Li S. & Montgomery D. Decaying two-dimensional turbulence with rigid walls *Phys. Lett. A* **218** 281–291 1996

[12] Linden P.F., Boubnov B.M. & Dalziel S.B. Source-sink turbulence in a rotating, stratified fluid, *J. Fluid Mech.* **298** 81–112 1995

[13] McWilliams J.C. The vortices of geostrophic turbulence, *J. Fluid Mech.* **219** 387–404 1990

[14] McWilliams J.C., Weiss J.B. & Yavneh I. Anisotropy and coherent vortex structures in planetary turbulence, *Science* **264** 410–413 1994

[15] Nielsen A.H., Rasmussen J.J. & Schmidt M.R. Formation and dynamics of dipolar vortices, *Proceedings of the International Workshop on Vortex Dynamics in Geophysical Flows*, Castro Marina, Italy, June 22–26, 1998

[16] Orszag S.A. & Patera A.T. Secondary instability of wall-bounded shear flows *J. Fluid Mech.* **128** 347–385 1983

[17] Pedlosky J. *Geophysical Fluid Dynamics* Springer-Verlag, New York, 1987

[18] Sutyrin G.G., McWilliams J.C. & Saravanan R. Co-rotating stationary states and vertical alignment of geostrophic vortices with thin cores, *J. Fluid Mech.* **357** 321–349 1998

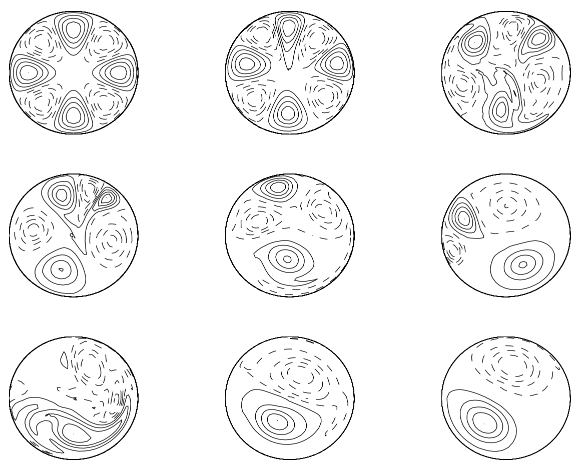

Figure 1: Contours of potential vorticity in the two-dimensional case $\beta = 0$ and with the initial condition given for $\psi = \psi_0$ by equation(12) where $r_0^{(4)}, r_0^{(1)}$ are chosen to give zero potential vorticity at the cylinder wall. In this and all succeeding figures the panels read in time order from left to right and then from top to bottom. The times are $t = 0, 40, 80, \ldots, 320$. Negative potential vorticity is shown dashed.

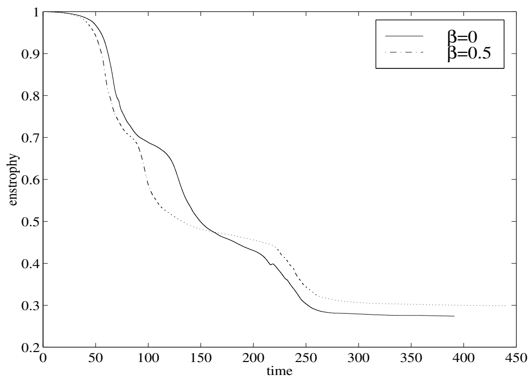

Figure 2: The enstrophy as a function of time for the initial condition $\psi = \psi_0 h(z)$ where ψ_0 is of the form (12) and where $r_0^{(4)}, r_0^{(1)}$ are chosen to give zero potential vorticity at the cylinder wall. The case with variation in the vertical ($\beta = 0.5$) is shown as (-.-.) while the two-dimensional case ($\beta = 0$) is shown with a solid curve.

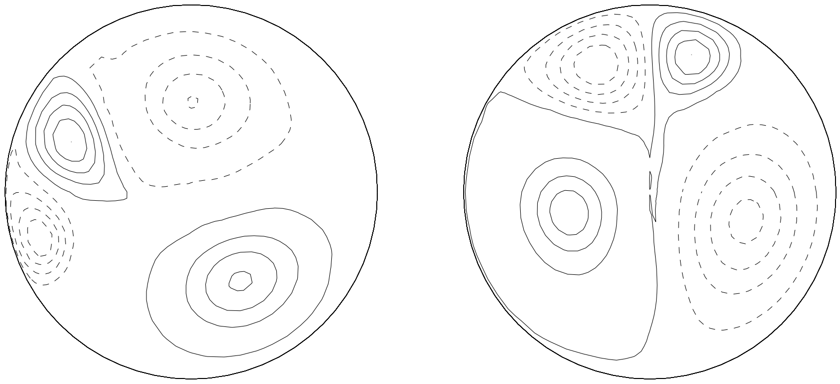

$\beta = 0$ $\beta = 0.5$

Figure 3: Contours of potential vorticity at mid-depth for the two cases described in Figure 2 at time $t = 200$. At this depth the quadrupole structures are very similar in the two cases, although there is clearly a phase difference.

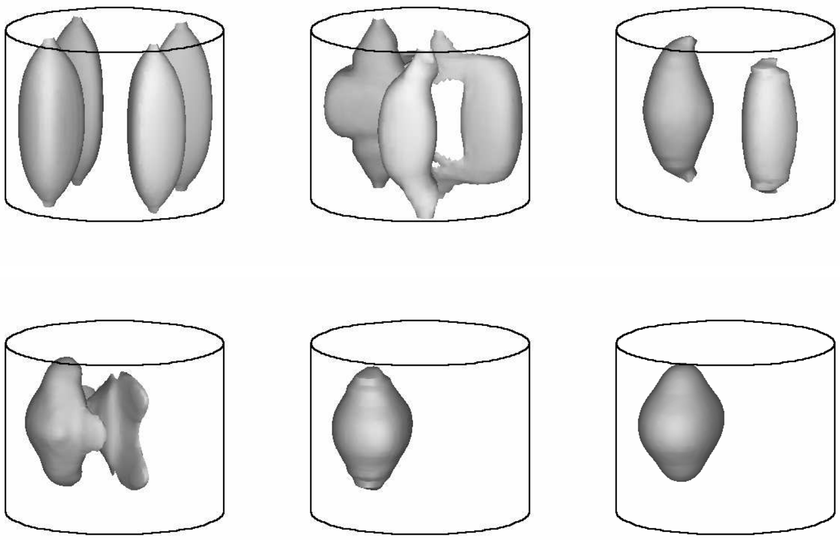

Figure 4: Contours of potential vorticity (one fifth the maximum initial positive value) for times $t = 0, 80, 160, \ldots, 400$ for the $\beta = 0.5$ case of Figures 2 and 3. Only positive contours are shown: as the negative contours show similar qualitative and quantitative behaviour the first frame in fact corresponds to an octopole, the third frame to a quadrupole and the final two frames to a dipole.

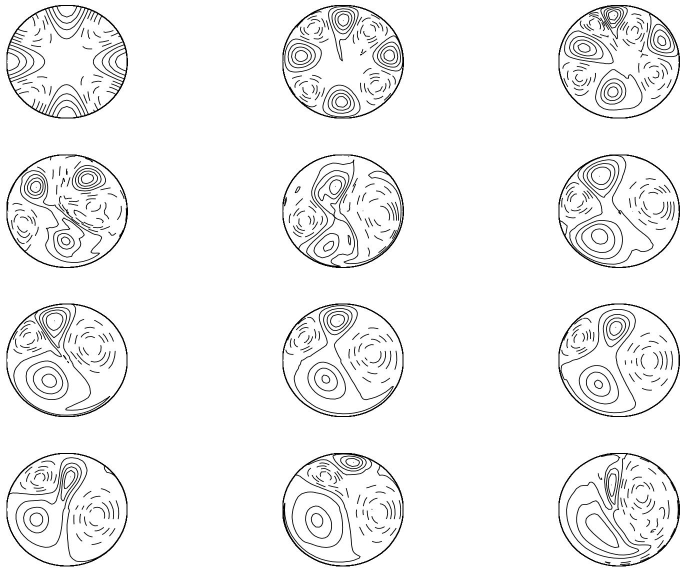

Figure 5: Contours of potential vorticity at mid-depth for the initial condition $\psi = \psi_0 h(z)$ where ψ_0 is given by (12) and where $r_0^{(4)}, r_0^{(1)}$ are chosen to give maximum potential vorticity at the cylinder wall. Here $\beta = 0.5$, and results are shown for times $t = 0, 40, ..., 440$. Note the persistence of the quadrupole state over the period $t \approx 240$ until $t \approx 400$ with the final breakup to a dipole form in the last two panels.

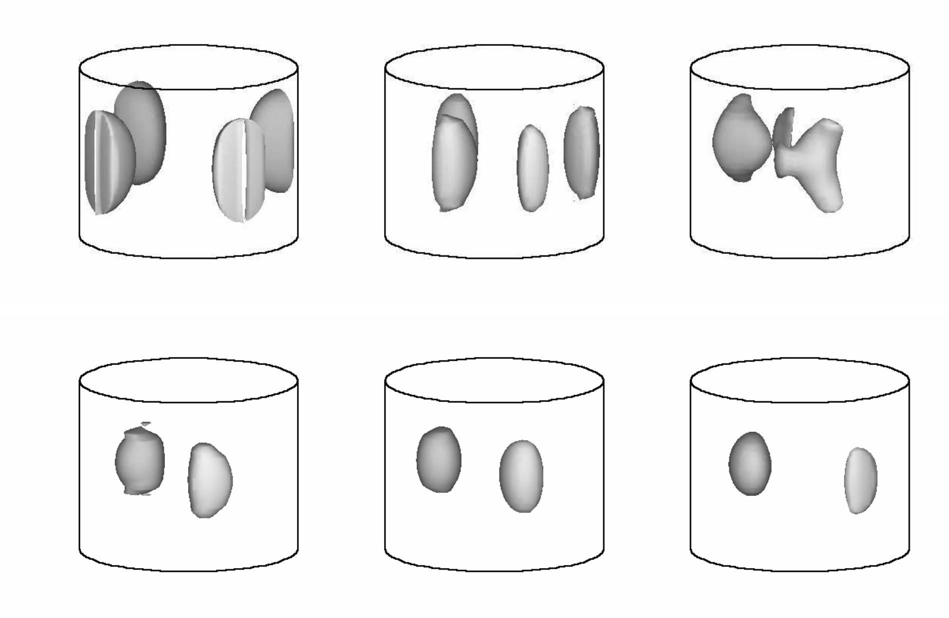

Figure 6: Contours of potential vorticity (one fifth the maximum initial positive value) for times $t = 0, 80, 160, \ldots, 400$ for the $\beta = 0.5$ case of Figure 5.

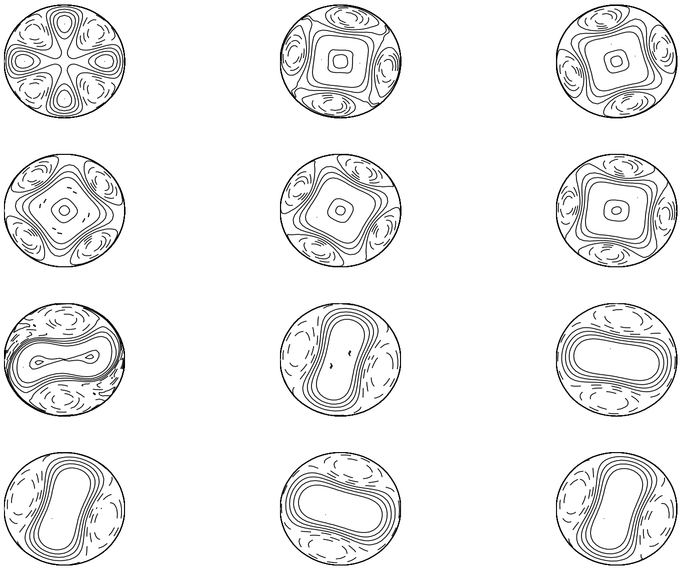

Figure 7: Contours of potential vorticity at mid-depth for the initial condition $\psi = \psi_0 h(z)$ where ψ_0 is given by 13 and where $r_0^{(4)}, r_0^{(1)}$ are chosen to give zero potential vorticity at the cylinder wall. Here $\beta = 0.5$, and results are shown for times $t = 0, 40, ..., 440$.

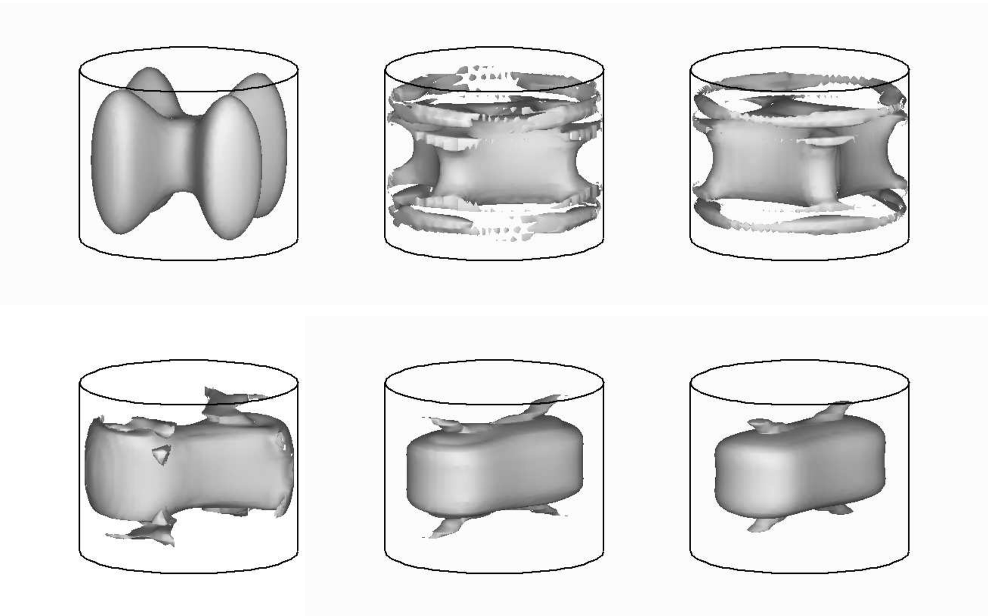

Figure 8: Contours of potential vorticity (one fifth the maximum initial positive value) for times $t = 0, 80, 160, \ldots, 400$ for the $\beta = 0.5$ case of Figure 7.